

Metallicity Calibration and Photometric Parallax Estimation: II. SDSS photometry

S. Tunçel Güçtekin¹ • S. Bilir² • S. Karaali² •
O. Plevne¹ • S. Ak² • T. Ak² • Z. F. Bostancı²

Abstract We used the updated [Fe/H] abundances of 168 F-G type dwarfs and calibrated them to a third order polynomial in terms of reduced ultraviolet excess, $\delta_{0.41}$ defined with *ugr* data in the SDSS. We estimated the M_g absolute magnitudes for the same stars via the re-reduced *Hipparcos* parallaxes and calibrated the absolute magnitude offsets, ΔM_g , relative to the intrinsic sequence of Hyades to a third order polynomial in terms of $\delta_{0.41}$. The ranges of the calibrations are $-2 < [\text{Fe}/\text{H}] \leq 0.3$ dex and $4 < M_g \leq 6$ mag. The

S. Tunçel Güçtekin

¹Istanbul University, Graduate School of Science and Engineering, Department of Astronomy and Space Sciences, 34116, Beyazit, Istanbul, Turkey

S. Bilir

²Istanbul University, Faculty of Science, Department of Astronomy and Space Sciences, 34119 University, Istanbul, Turkey

S. Karaali

²Istanbul University, Faculty of Science, Department of Astronomy and Space Sciences, 34119 University, Istanbul, Turkey

O. Plevne

¹Istanbul University, Graduate School of Science and Engineering, Department of Astronomy and Space Sciences, 34116, Beyazit, Istanbul, Turkey

S. Ak

²Istanbul University, Faculty of Science, Department of Astronomy and Space Sciences, 34119 University, Istanbul, Turkey

T. Ak

²Istanbul University, Faculty of Science, Department of Astronomy and Space Sciences, 34119 University, Istanbul, Turkey

Z. F. Bostancı

²Istanbul University, Faculty of Science, Department of Astronomy and Space Sciences, 34119 University, Istanbul, Turkey

mean of the residuals and the corresponding standard deviation for the metallicity calibration are 0 and 0.137 mag; while, for the absolute magnitude calibration they are 0 and 0.179 mag, respectively. We applied our procedures to 23,414 dwarf stars in the Galactic field with the Galactic coordinates $85^\circ \leq b \leq 90^\circ$, $0^\circ \leq l \leq 360^\circ$ and size 78 deg^2 . We estimated absolute magnitude M_g dependent vertical metallicity gradients as a function of vertical distance Z . The gradients are deep in the range of $0 < Z \leq 5 \text{ kpc}$, while they are very small positive numbers beyond $Z = 5 \text{ kpc}$. All dwarfs with $5 < M_g \leq 6$ mag are thin-disc stars and their distribution shows a mode at $(g - r)_0 \approx 0.38$ mag, while the absolute magnitudes $4 < M_g \leq 5$ are dominated by thick disc and halo stars, i.e. the apparently bright ones ($g_0 \leq 18$ mag) are thick-disc stars with a mode at $(g - r)_0 \sim 0.38$ mag, while the halo population is significant in the faint stars ($g_0 > 18$ mag).

Keywords Galaxy: disc, Galaxy: halo, stars: abundances, stars: distances

1 Introduction

Metallicity distribution of stars in our Galaxy has been used as an indicator for understanding its formation. The pioneer work related to the formation of our Milky Way Galaxy is the one of Eggen, Lynden-Bell & Sandage (1962, hereafter ELS) who argued that the Galaxy collapsed in a free-fall time, i.e. 2×10^8 Gyr. However, this argument was in contradiction with the metallicity gradients observed at least in some of the components of the Galaxy, which indicate a dissipative collapse in a much longer time-scale than the predicted one of ELS. Many studies confirmed this new idea (cf. Karaali et al. 2004; Bilir et al. 2006, 2008a, and references therein).

Additionally, we know that at least some of the components of the Galaxy were formed from merger or accretion of numerous fragments, such as dwarf-type galaxies (cf. Searle & Zinn 1978; Freeman & Bland-Hawthorn 2002). A positive iron abundance gradient in the increasing vertical direction of the Galactic halo is a typical feature for the mentioned mergers and accretions. Despite these studies, the researchers still investigate the formation -and evolution- of the Galaxy by using the recent data, which are more accurate.

Metallicity of a star can be determined spectroscopically or photometrically. The first procedure requires high-resolution spectra, hence it can be applied only to nearby stars. While the second one is valid for distant stars as well. The invent of large telescopes which provide high resolution increased the accuracy of metallicity estimation.

The distance to a star is important in the kinematical investigation of the Galaxy. It can be estimated by using trigonometric or photometric parallaxes. The estimation of the trigonometric parallax of a star is limited with distance, i.e. it can be applied only to nearby stars. While, photometric parallax can be applied to distant stars as well. The main source for the trigonometric parallax is the *Hipparcos* data (ESA 1997; van Leeuwen 2007). Photometric parallax of a star can be provided by combination of its apparent and absolute magnitudes (cf. Bilir et al. 2008b, 2009). However, estimation of the absolute magnitude of a star is another problem. The procedure usually used for its estimation is based on its offset from a standard sequence, such as the absolute magnitude-colour diagram of the Hyades cluster. Examples can be found in Laird et al. (1988); Nissen & Schuster (1991); Karaali et al. (2003a, 2005); Karataş & Schuster (2006). The procedure of Ivezić et al. (2008) is different than the cited ones, i.e. they calibrated the [Fe/H] to a third order polynomial in terms of $(g - r)_0$, $(u - g)_0$ and their combination. Also, they calibrated the absolute magnitude M_r instead of M_g . Additionally, the standard sequence used in their calibration consists of a theoretical third order polynomial of the colour $(g - i)_0$. Alternative methods are given in some studies in the literature (Phleps et al. 2000; Chen et al. 2001; Siegel et al. 2002).

In our previous study (Tunçel Güçtekin et al. 2016, hereafter Paper I), we used the *UBV* data and calibrated the iron abundance [Fe/H] and absolute magnitude offset ΔM_V in terms of the reduced ultraviolet (UV) excess, $\delta_{0.6}(U - B)$. In this study, our calibrations will be based on the *ugr* data of Sloan Digital Sky Survey (SDSS, York et al. 2000) which has a wider application area, i.e. [Fe/H] and ΔM_g will be calibrated in terms of ultra-violet excess in the *ugr* system, where

M_g is the absolute magnitude of a star corresponding to the *g*-band. However, here we have a difficulty, i.e. the spaces occupied by stars observed with *Hipparcos* (ESA 1997) and SDSS are different. The solution of this problem is to transform the *UBV* data of the sample stars in Paper I to the *ugr* data and adopt the same procedure for our purpose. Thus, we should extend our calibrations to stars observed with SDSS at larger distances. Also, the application of our new calibrations will be carried out in this study. We organized the paper as follows. The data are presented in Section 2. The procedure and its application are given in Section 3 and Section 4, respectively. Finally, Section 5 is devoted to Summary and Discussion.

2 Data

The data consist of g_0 magnitudes, $(g - r)_0$ and $(u - g)_0$ colours, [Fe/H] iron abundances, M_g absolute magnitudes of a sample of 168 stars; and the $(u - g)_0 \times (g - r)_0$ two-colour diagram and $M_g \times (g - r)_0$ sequence of the Hyades cluster, which are provided as explained in the following. The subscript “0” denotes the de-reddened magnitudes and colours. The sample is the same as in Paper I, i.e. they are F and G type dwarfs with $5310 < T_{eff}(K) < 7300$ and $\log g > 4$ (cgs). Hence, their iron abundances are identical with the ones used in Paper I.

We used the transformation equations of Chonis & Gaskell (2008) (Eqs. 1-5) and obtained their inverse ones (Eqs. 6-8) as in the following:

$$B_0 = g_0 + 0.327(g - r)_0 + 0.216. \quad (1)$$

$$V_0 = g_0 - 0.587(g - r)_0 - 0.011. \quad (2)$$

$$R_0 = r_0 - 0.272(r - i)_0 - 0.159. \quad (3)$$

$$I_0 = i_0 - 0.337(r - i)_0 - 0.370. \quad (4)$$

$$U_0 = u_0 - 0.854. \quad (5)$$

$$g_0 = V_0 + 0.642(B - V). \quad (6)$$

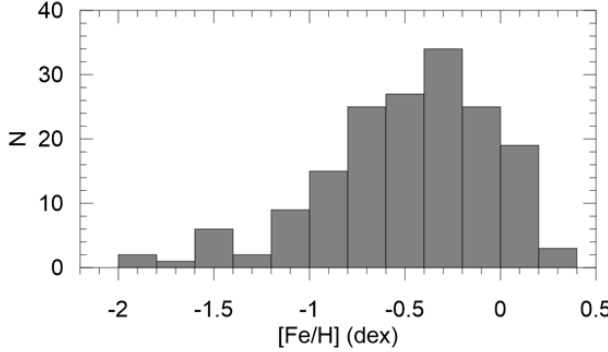


Fig. 1 Metallicity distribution for 168 sample stars.

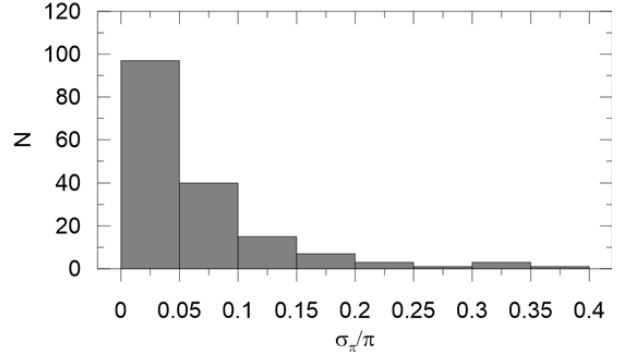


Fig. 2 Distribution of the relative parallax errors for 168 sample stars.

$$(u-g)_0 = (U-B)_0 + 0.358(B-V)_0 + 0.989. \quad (7)$$

$$(g-r)_0 = 1.094(B-V)_0 - 0.248. \quad (8)$$

The g_0 , $(g-r)_0$ and $(u-g)_0$ data are given in Table 1. The range of the $(g-r)_0$ colour index is $0.15 < (g-r)_0 < 0.50$ mag. The iron abundances of the sample stars which are taken from Paper I (originally from Bensby et al. 2014; Nissen & Schuster 2010; Reddy et al. 2006; Venn et al. 2004) are also given in Table 1 and their distribution is presented in Fig. 1. The trigonometric parallaxes are provided from the re-reduced *Hipparcos* catalogue (van Leeuwen 2007); 84% of their relative parallax errors are less than 0.1 (Fig. 2). The absolute magnitudes are evaluated by the following Pogson equation:

$$g_0 - M_g = 5 \times \log d - 5. \quad (9)$$

where d is the distance to the star estimated via its trigonometric parallax. The distribution of absolute magnitudes are shown in Fig. 3. The range of the absolute magnitudes is $3.5 \leq M_g \leq 6.5$ mag.

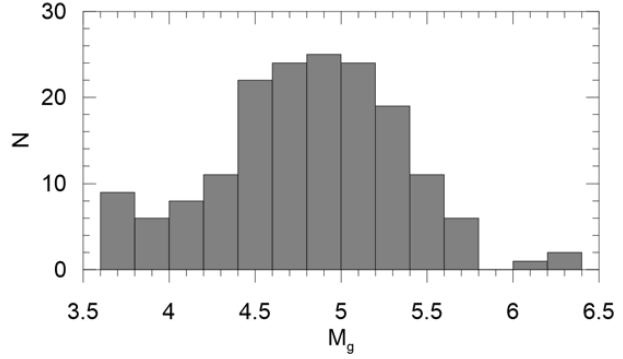


Fig. 3 Original absolute magnitude distribution for 168 sample stars.

The two-colour diagram $(u-g)_0 \times (g-r)_0$ and the absolute magnitude-colour diagram $M_g \times (g-r)_0$ of the Hyades cluster used in our calibrations are provided from Karaali et al. (2003a) and Sandage (1969), respectively, by transformation of their two-colour and absolute magnitude-colour diagrams from the *UBV* system to the *ugr* one. We should emphasize that the M_V absolute magnitudes had been updated by considering the re-reduced *Hipparcos* (van Leeuwen 2007) trigonometric parallaxes before the necessary transformations. The results are given in Table 2, Fig. 4 and Fig. 5. The equations of the $(u-g)_0$ colour index and M_g absolute magnitude for the Hyades cluster in terms of $(g-r)_0$ colour index are as follows:

$$(u-g)_0 = 0.839 + 2.756(g-r)_0 - 10.744(g-r)_0^2 \quad (10) \\ + 24.252(g-r)_0^3 - 20.585(g-r)_0^4 + 5.961(g-r)_0^5.$$

$$M_g = 2.343 + 0.575(g-r)_0 + 32.996(g-r)_0^2 \quad (11) \\ - 71.036(g-r)_0^3 + 62.039(g-r)_0^4 - 19.128(g-r)_0^5.$$

Table 1 Atmospheric and photometric parameters for 168 sample stars used in the calibrations. The columns give: ID, Hipparcos number, equatorial coordinates (α, δ), trigonometric parallax (π), effective temperature (T_{eff}), surface gravity ($\log g$), iron abundance [Fe/H], apparent magnitude (V_0), colour indices ($(U - B)_0, (B - V)_0$), apparent magnitude (g_0), and colour indices ($(u - g)_0, (g - r)_0$).

ID	Hip	α_{2000} (hh:mm:ss.ss)	δ_{2000} (dd:mm:ss.s)	π (mas)	T_{eff} (K)	$\log g$ (cgs)	[Fe/H] (dex)	V_0 (mag)	$(U - B)_0$ (mag)	$(B - V)_0$ (mag)	g_0 (mag)	$(u - g)_0$ (mag)	$(g - r)_0$ (mag)
1	493	00 05 54.70	+18 14 06.0	26.93	5826	4.36	-0.29	7.435	0.036	0.555	7.656	1.224	0.359
2	910	00 11 15.86	-15 28 04.7	53.34	6289	4.17	-0.33	4.886	-0.016	0.489	5.065	1.148	0.287
3	1599	00 20 04.26	-64 52 29.3	116.46	5932	4.33	-0.19	4.225	0.017	0.571	4.457	1.210	0.377
4	1976	00 25 01.42	-30 41 51.7	21.27	5982	4.32	+0.19	7.548	0.152	0.611	7.805	1.360	0.420
5	2711	00 34 27.83	-52 22 23.1	39.24	6499	4.22	+0.06	5.563	-0.017	0.464	5.726	1.138	0.260
6	3182	00 40 32.24	-29 52 05.8	16.76	5643	4.32	-0.29	8.695	0.084	0.627	8.963	1.297	0.438
7	3479	00 44 26.65	-26 30 56.4	30.89	5563	4.40	-0.26	7.777	0.155	0.663	8.068	1.381	0.477
8	3497	00 44 39.27	-65 38 58.3	45.34	5638	4.41	-0.32	6.538	0.106	0.652	6.822	1.328	0.465
9	3704	00 47 30.75	-36 56 24.7	20.51	6078	4.40	-0.35	7.819	-0.044	0.536	8.028	1.137	0.338
10	3909	00 50 07.59	-10 38 39.6	63.48	6352	4.45	-0.03	5.178	-0.005	0.507	5.368	1.166	0.307
11	4544	00 58 11.69	+80 06 49.3	9.23	5832	4.51	-0.87	9.630	-0.135	0.492	9.811	1.030	0.290
12	4892	01 02 49.72	-37 18 58.2	16.48	5994	4.42	-0.29	8.501	0.004	0.575	8.735	1.199	0.381
13	5163	01 06 05.15	+01 42 23.1	10.84	5547	4.63	-0.74	9.416	-0.007	0.584	9.656	1.191	0.391
14	5301	01 07 48.66	-08 14 01.3	18.23	5686	4.39	-0.11	8.384	0.157	0.632	8.655	1.372	0.443
15	5862	01 15 11.12	-45 31 54.0	66.16	6145	4.24	+0.17	4.954	0.097	0.570	5.185	1.290	0.376
16	6159	01 18 59.99	-08 56 22.2	15.35	5653	4.56	-0.67	8.862	-0.027	0.583	9.101	1.171	0.390
17	7217	01 32 57.60	+23 41 44.0	14.60	5550	4.20	-0.48	8.960	0.043	0.598	9.209	1.246	0.406
18	7459	01 36 05.80	-61 05 03.0	10.87	5759	4.31	-1.23	10.07	-0.167	0.520	10.269	1.008	0.321
19	7978	01 42 29.32	-53 44 27.0	57.36	6219	4.41	+0.05	5.531	-0.006	0.527	5.734	1.172	0.329
20	8859	01 53 57.68	+10 36 50.5	24.12	6420	4.21	-0.30	6.730	-0.062	0.444	6.880	1.086	0.238
21	9085	01 56 59.98	-51 45 58.5	37.22	6334	4.29	-0.26	6.088	-0.062	0.477	6.259	1.098	0.274
22	10449	02 14 40.30	-01 12 05.1	15.87	5566	4.64	-0.87	9.055	-0.077	0.571	9.287	1.116	0.377
23	10652	02 17 07.14	+21 34 00.5	15.93	5499	4.58	-0.67	8.954	-0.008	0.592	9.199	1.193	0.400
24	12294	02 38 21.50	+02 26 44.4	5.82	6069	4.58	-0.95	10.47	-0.171	0.443	10.619	0.977	0.237
25	12306	02 38 27.86	+30 48 59.9	29.17	5832	4.44	-0.52	7.306	-0.015	0.569	7.536	1.178	0.374
26	12444	02 40 12.42	-09 27 10.4	45.96	6383	4.41	+0.09	5.766	-0.013	0.517	5.963	1.161	0.318
27	12653	02 42 33.47	-50 48 01.1	58.25	6375	4.73	+0.27	5.394	0.073	0.553	5.614	1.260	0.357
28	12777	02 44 12.00	+49 13 42.0	89.87	5309	4.30	-0.02	4.090	-0.009	0.482	4.264	1.153	0.279
29	12889	02 45 41.01	-38 09 31.4	20.16	5999	4.23	-0.13	7.625	0.043	0.576	7.860	1.238	0.382
30	13366	02 51 58.36	+11 22 11.9	16.39	5856	4.26	-0.69	8.234	-0.096	0.499	8.419	1.072	0.298
31	14241	03 03 38.96	-05 39 58.7	28.54	5430	4.33	-0.45	8.048	0.108	0.658	8.335	1.333	0.472
32	15131	03 15 06.39	-45 39 53.4	41.34	5985	4.54	-0.43	6.748	-0.023	0.576	6.983	1.172	0.382
33	15158	03 15 22.52	-01 10 43.1	10.55	6191	4.18	-0.06	8.460	0.009	0.501	8.647	1.177	0.300
34	15381	03 18 19.98	+18 10 17.8	20.16	5882	4.24	+0.08	7.472	0.154	0.598	7.721	1.357	0.406
35	16169	03 28 21.08	-06 31 51.3	21.38	5650	4.34	-0.57	8.210	0.022	0.612	8.468	1.230	0.422
36	17147	03 40 22.06	-03 13 01.1	39.12	5970	4.52	-0.81	6.664	-0.092	0.532	6.871	1.087	0.334
37	22632	04 52 09.91	-27 03 51.0	15.00	5909	4.22	-1.62	9.106	-0.196	0.481	9.280	0.965	0.278
38	23555	05 03 53.95	-41 44 41.8	31.50	6466	4.64	+0.22	6.296	0.039	0.528	6.500	1.217	0.330
39	23688	05 05 28.70	+40 15 26.0	8.79	6293	4.41	-0.89	9.647	-0.163	0.416	9.779	0.975	0.207
40	24030	05 09 56.96	+05 33 26.7	8.66	5738	4.64	-1.00	9.648	-0.147	0.497	9.832	1.020	0.296
41	25860	05 31 13.78	+15 46 24.4	20.07	5543	4.56	-0.35	8.506	0.088	0.627	8.774	1.301	0.438
42	26617	05 39 27.44	+03 57 02.7	8.79	5429	4.67	-0.75	10.116	-0.025	0.554	10.337	1.162	0.358
43	27072	05 44 27.79	-22 26 54.2	112.02	6323	4.16	-0.02	3.587	-0.008	0.480	3.760	1.153	0.277
44	28403	05 59 55.79	-37 03 24.2	19.64	5668	4.31	-0.33	8.575	0.046	0.620	8.838	1.257	0.430
45	28671	06 03 14.86	+19 21 38.7	16.81	5396	4.39	-1.11	9.260	-0.055	0.602	9.511	1.150	0.411
46	29432	06 12 00.60	+06 46 59.0	42.55	5726	4.58	-0.16	6.826	0.119	0.625	7.092	1.332	0.436
47	31188	06 32 37.99	-06 29 18.5	16.79	5789	4.54	-0.59	8.514	-0.094	0.525	8.716	1.083	0.326
48	33582	06 58 38.54	-00 28 49.7	12.56	5773	4.11	-0.62	8.987	-0.024	0.569	9.217	1.169	0.374
49	34017	07 03 30.46	+29 20 13.5	52.27	5920	4.42	-0.12	5.921	0.058	0.588	6.163	1.258	0.395
50	34511	07 09 04.96	+15 25 17.7	21.64	5789	4.44	-0.11	7.981	0.116	0.614	8.240	1.325	0.424
51	35139	07 15 50.80	-13 02 58.1	30.95	5771	4.47	-0.52	7.749	-0.018	0.605	8.002	1.188	0.414
52	36491	07 30 29.02	+18 57 40.6	20.20	5869	4.31	-0.95	8.482	-0.120	0.514	8.677	1.053	0.314
53	36849	07 34 35.11	+16 54 04.0	12.37	6012	4.16	-0.84	8.922	-0.116	0.501	9.109	1.052	0.300
54	37419	07 40 54.38	-26 21 48.6	19.16	5715	4.38	-0.33	8.655	0.064	0.616	8.915	1.274	0.426
55	38541	07 53 33.12	+30 36 18.3	34.30	5316	4.60	-1.84	8.288	-0.128	0.615	8.548	1.081	0.425
56	38769	07 56 10.20	+50 32 27.3	11.56	5726	4.15	-0.79	8.780	-0.072	0.504	8.969	1.097	0.303
57	40118	08 11 38.64	+32 27 25.7	45.90	5484	4.58	-0.47	6.817	0.125	0.676	7.116	1.356	0.492
58	40778	08 19 22.60	+54 05 10.0	10.35	6006	4.23	-1.55	9.699	-0.222	0.467	9.864	0.934	0.263
59	41484	08 27 36.80	+45 39 11.0	44.94	5703	4.46	-0.08	6.312	0.118	0.623	6.577	1.330	0.434
60	42356	08 38 08.51	+26 02 56.3	22.91	5962	4.42	+0.17	7.560	0.131	0.626	7.827	1.344	0.437
61	43595	08 52 44.51	+22 33 30.2	7.87	5506	4.67	-0.84	10.789	-0.049	0.587	11.031	1.150	0.394
62	43726	08 54 17.90	-05 26 04.0	57.52	5763	4.37	+0.01	6.007	0.211	0.665	6.299	1.438	0.480
63	44116	08 59 06.00	-00 37 26.0	12.70	6275	4.10	-0.58	8.456	-0.109	0.432	8.598	1.035	0.225
64	44713	09 06 38.83	-43 29 31.1	26.83	5823	4.34	+0.14	7.261	0.191	0.651	7.544	1.413	0.464
65	44811	09 07 56.60	-50 28 57.0	24.53	5824	4.45	-0.64	7.622	-0.063	0.532	7.829	1.116	0.334
66	47048	09 35 16.70	-49 07 48.9	10.26	6630	4.12	-0.50	8.451	-0.118	0.366	8.551	1.002	0.152
67	47174	09 36 49.50	+57 54 41.0	11.99	5603	4.33	-0.45	9.940	0.025	0.623	10.205	1.237	0.434
68	48209	09 49 42.82	+65 18 15.0	13.10	5415	4.64	-0.65	9.601	0.078	0.643	9.879	1.297	0.455
69	49285	10 03 37.38	-29 02 36.0	21.13	5520	4.29	-0.21	8.073	0.191	0.668	8.367	1.419	0.483
70	49615	10 07 33.80	-06 26 21.0	21.25	6019	4.29	-0.43	7.703	-0.064	0.504	7.892	1.105	0.303
71	49793	10 09 49.58	-36 45 14.9	22.58	5764	4.33	-0						

ID	Hip	α_{2000} (hh:mm:ss.ss)	δ_{2000} (dd:mm:ss.s)	π (mas)	T_{eff} (K)	$\log g$ (cgs)	[Fe/H] (dex)	V_o (mag)	$(U - B)_o$ (mag)	$(B - V)_o$ (mag)	g_o (mag)	$(u - g)_o$ (mag)	$(g - r)_o$ (mag)
81	54924	11 14 49.93	-23 38 47.9	15.02	5682	4.34	-0.80	9.018	-0.008	0.568	9.248	1.184	0.373
82	55592	11 23 16.23	+19 53 37.7	8.35	5995	4.14	-1.02	9.942	-0.147	0.470	10.109	1.010	0.266
83	55761	11 25 31.80	+42 37 58.0	22.95	5741	4.35	-0.62	7.847	-0.043	0.536	8.056	1.138	0.338
84	56664	11 37 08.12	-39 28 12.0	9.45	6364	4.07	-0.68	8.636	-0.109	0.412	8.766	1.027	0.203
85	57017	11 41 22.48	-26 40 01.9	18.78	6380	4.35	-0.43	7.508	-0.065	0.463	7.670	1.090	0.259
86	57265	11 44 35.70	+25 32 12.0	6.25	5928	4.23	-0.93	10.318	-0.143	0.462	10.48	1.011	0.257
87	57443	11 46 31.10	-40 30 01.0	108.45	5524	4.29	-0.35	4.879	0.098	0.662	5.169	1.324	0.476
88	57450	11 46 35.15	+50 52 54.7	12.85	5315	4.74	-1.50	9.902	-0.154	0.555	10.123	1.034	0.359
89	58843	12 04 05.56	+03 20 26.7	14.24	5726	4.41	-0.84	9.194	-0.059	0.579	9.431	1.137	0.385
90	58950	12 05 13.41	-28 43 02.0	27.85	5686	4.45	-0.19	7.757	0.134	0.642	8.034	1.353	0.454
91	59380	12 10 57.93	-46 19 19.1	27.31	5901	4.38	-0.58	7.502	-0.059	0.554	7.723	1.128	0.358
92	61053	12 30 50.10	+53 04 36.0	45.92	6060	4.35	-0.11	6.193	0.013	0.545	6.408	1.197	0.348
93	61619	12 37 39.13	+38 41 03.7	17.81	6429	4.26	+0.04	7.338	-0.023	0.476	7.509	1.136	0.273
94	62108	12 43 43.22	-44 40 31.6	8.17	6293	4.37	-1.53	9.841	-0.176	0.441	9.989	0.971	0.234
95	62207	12 44 59.40	+39 16 44.0	57.55	5795	4.15	-0.59	5.945	-0.045	0.546	6.161	1.139	0.349
96	62809	12 52 11.64	-56 34 28.0	20.67	5658	4.38	-0.77	8.424	-0.032	0.596	8.672	1.170	0.404
97	64345	13 11 21.40	+09 37 33.5	16.88	5598	4.37	-0.60	8.718	0.047	0.613	8.977	1.255	0.423
98	64394	13 11 52.40	+27 52 41.0	109.54	6029	4.38	+0.03	4.228	0.067	0.570	4.459	1.260	0.376
99	64698	13 15 36.97	+09 00 57.7	18.48	5624	4.35	-0.13	8.425	0.164	0.652	8.709	1.386	0.465
100	64747	13 16 11.25	+35 53 09.1	21.87	5718	4.47	-0.21	8.271	0.118	0.637	8.545	1.335	0.449
101	65418	13 24 30.60	+20 27 22.0	3.12	6043	4.18	-1.56	12.138	-0.186	0.433	12.281	0.958	0.226
102	66238	13 34 32.65	-38 54 26.0	33.27	5660	4.42	-0.22	7.279	0.117	0.665	7.571	1.344	0.480
103	67655	13 51 40.40	-57 26 08.0	39.42	5396	4.38	-0.93	7.941	-0.002	0.653	8.225	1.221	0.466
104	67863	13 53 58.12	-46 32 19.5	16.70	5692	4.35	-0.76	9.004	-0.055	0.593	9.250	1.146	0.401
105	68030	13 55 50.00	+14 03 23.0	40.22	6081	4.40	-0.38	6.151	-0.087	0.498	6.336	1.080	0.297
106	70319	14 23 15.30	+01 14 30.0	58.17	5597	4.44	-0.41	6.242	0.081	0.634	6.514	1.297	0.446
107	70681	14 27 24.91	-18 24 40.4	21.04	5484	4.48	-1.30	9.259	-0.113	0.583	9.498	1.085	0.390
108	70829	14 29 03.26	-46 44 28.0	19.18	5471	4.47	-0.67	8.903	0.084	0.673	9.200	1.314	0.488
109	71076	14 32 04.50	+18 50 10.0	17.24	6038	4.22	-0.39	7.787	-0.085	0.493	7.969	1.080	0.291
110	71735	14 40 28.26	-57 01 46.4	37.71	5513	4.43	-0.35	7.348	0.141	0.658	7.635	1.366	0.472
111	72407	14 48 18.70	+58 54 36.1	10.65	5567	4.56	-0.54	9.750	0.071	0.617	10.011	1.281	0.427
112	72673	14 51 31.72	-60 55 50.8	20.06	6374	4.29	-0.56	7.117	-0.117	0.431	7.259	1.026	0.224
113	74067	15 08 12.57	-07 54 47.5	26.62	5695	4.38	-0.81	7.969	-0.057	0.580	8.206	1.140	0.387
114	75181	15 21 48.15	-48 19 03.5	67.51	5698	4.46	-0.32	5.639	0.066	0.635	5.912	1.282	0.447
115	78640	16 03 13.30	+42 14 46.6	8.41	6069	4.30	-1.43	9.835	-0.202	0.468	10.000	0.955	0.264
116	81520	16 39 04.14	-58 15 29.5	44.54	5746	4.62	-0.44	7.002	0.025	0.609	7.258	1.232	0.418
117	81681	16 41 08.21	-02 51 26.2	33.82	5565	4.52	-0.38	7.160	0.050	0.604	7.413	1.255	0.413
118	83229	17 00 31.65	-57 17 49.6	32.77	5865	4.41	-0.49	6.987	-0.024	0.568	7.217	1.168	0.373
119	83489	17 03 49.15	+17 11 21.1	13.43	5722	4.28	-0.29	9.078	0.088	0.635	9.351	1.304	0.447
120	84988	17 22 12.65	-75 20 53.3	35.67	5686	4.25	-0.70	6.977	-0.016	0.593	7.223	1.185	0.401
121	85007	17 22 27.65	+24 52 46.0	34.12	6064	4.32	-0.39	6.851	-0.068	0.505	7.040	1.102	0.304
122	85042	17 22 51.29	-02 23 17.4	51.22	5648	4.46	0.00	6.217	0.220	0.659	6.505	1.445	0.473
123	86013	17 34 43.06	+06 00 51.6	19.38	5760	4.30	-0.81	8.353	-0.059	0.558	8.576	1.130	0.362
124	86321	17 38 15.61	+18 33 25.5	8.38	5760	4.59	-0.87	9.724	-0.117	0.465	9.888	1.038	0.261
125	87062	17 47 28.00	-08 46 48.0	9.59	6027	4.32	-1.49	10.266	-0.209	0.485	10.442	0.954	0.283
126	88945	18 09 21.38	+29 57 06.2	40.29	5869	4.62	+0.02	6.838	0.087	0.616	7.098	1.297	0.426
127	92270	18 48 16.40	+23 30 53.1	34.78	6376	4.23	-0.05	6.098	0.015	0.494	6.280	1.181	0.292
128	92532	18 51 25.20	+38 37 36.0	32.72	5825	4.30	-0.56	7.138	-0.048	0.536	7.347	1.133	0.338
129	92781	18 54 23.20	-04 36 18.6	14.59	5765	4.33	-0.69	9.000	-0.067	0.561	9.225	1.123	0.366
130	93185	18 58 51.00	+30 10 50.3	41.94	5864	4.54	-0.29	6.775	-0.004	0.575	7.009	1.191	0.381
131	94129	19 09 39.24	-21 28 10.8	17.60	5630	4.35	-0.27	8.171	0.121	0.617	8.432	1.331	0.427
132	94645	19 15 33.23	-24 10 45.7	36.30	6365	4.56	+0.24	6.232	0.065	0.533	6.439	1.245	0.335
133	96124	19 32 40.33	-28 01 11.3	36.72	5577	4.47	-0.22	7.129	0.150	0.664	7.420	1.377	0.478
134	96258	19 34 19.79	+51 14 11.8	39.82	6380	4.15	-0.03	5.721	-0.012	0.464	5.884	1.143	0.260
135	98355	19 58 58.54	-46 05 17.0	19.11	6232	4.18	-0.62	7.445	-0.092	0.468	7.610	1.065	0.264
136	99139	20 07 36.91	-41 01 09.6	17.95	5612	4.32	-0.37	8.809	0.093	0.630	9.078	1.308	0.441
137	99938	20 16 38.08	-07 26 37.8	17.64	5732	4.48	-0.54	8.360	-0.031	0.566	8.588	1.161	0.371
138	100017	20 17 31.30	+66 51 13.0	56.92	5782	4.44	-0.19	5.854	0.045	0.567	6.083	1.237	0.372
139	100279	20 20 24.60	+06 01 53.0	10.46	5673	4.31	-0.72	10.039	-0.070	0.583	10.278	1.128	0.390
140	100568	20 23 35.85	-21 22 14.2	22.78	5800	4.48	-1.10	8.628	-0.139	0.541	8.840	1.044	0.344
141	100792	20 26 11.92	+09 27 00.4	17.00	6002	4.31	-1.11	8.310	-0.182	0.472	8.478	0.976	0.268
142	102018	20 40 22.33	-24 07 04.9	24.89	5933	4.12	+0.13	7.187	0.137	0.594	7.433	1.339	0.402
143	102046	20 49 49.38	-18 47 33.3	16.15	6009	4.13	-1.05	8.204	-0.137	0.486	8.381	1.026	0.284
144	102762	20 49 15.19	-20 37 50.8	17.11	5948	4.30	-0.04	8.070	0.067	0.575	8.304	1.262	0.381
145	102805	20 49 37.80	+12 32 42.0	32.66	6337	4.31	-0.32	5.990	-0.095	0.414	6.121	1.042	0.205
146	103458	20 57 40.07	-44 07 45.7	45.17	5843	4.53	-0.61	6.507	-0.045	0.582	6.746	1.152	0.389
147	103498	20 58 08.52	-48 12 13.5	18.95	5856	4.23	-1.11	8.271	-0.134	0.514	8.466	1.039	0.314
148	103897	21 03 06.10	+29 28 56.0	7.70	5607	4.39	-0.67	10.083	0.005	0.576	10.318	1.200	0.382
149	104659	21 11 59.03	+17 43 39.9	29.10	5973	4.35	-1.08	7.343	-0.164	0.502	7.530	1.005	0.301
150	107294	21 43 57.12	+27 23 24.0	9.03	5929	4.63	-1.14	9.993	-0.153	0.462	10.155	1.001	0.257
151	107877	21 51 24.61	-23 16 14.2	24.91	6355	4.20	-0.24	6.850	-0.049	0.477	7.021	1.111	0.274
152	108468	21											

Table 2 Photometric parameters for the stars in Hyades cluster. M_V and M_g are the absolute magnitudes in the UBV and ugr systems, respectively, the other symbols as in Table 1.

ID	Hip	V_o	$(U - B)_o$	$(B - V)_o$	M_V	g_o	$(u - g)_o$	$(g - r)_o$	M_g
1	18327	8.990	0.640	0.890	5.880	9.426	1.948	0.726	6.314
2	18946	10.130	1.030	1.070	6.960	10.682	2.402	0.923	7.516
3	19098	9.290	0.580	0.890	5.630	9.726	1.888	0.726	6.067
4	19148	7.850	0.100	0.600	4.540	8.100	1.304	0.408	4.789
5	19207	10.480	1.120	1.180	7.400	11.103	2.531	1.043	8.021
6	19263	9.940	0.890	0.990	6.410	10.441	2.233	0.835	6.910
7	19316	11.270	1.260	1.320	8.340	11.982	2.722	1.196	9.051
8	19504	6.620	-0.010	0.420	3.390	6.755	1.129	0.211	3.527
9	19781	8.460	0.240	0.700	5.130	8.774	1.480	0.518	5.448
10	19786	8.060	0.170	0.640	4.900	8.336	1.388	0.452	5.172
11	19793	8.090	0.200	0.660	4.710	8.379	1.425	0.474	4.998
12	19796	7.120	0.050	0.510	3.850	7.312	1.222	0.310	4.044
13	19808	10.750	1.180	1.180	7.880	11.373	2.591	1.043	8.505
14	20082	9.600	0.800	0.990	5.980	10.101	2.143	0.835	6.483
15	20146	8.450	0.310	0.730	5.120	8.784	1.560	0.551	5.451
16	20349	6.800	-0.030	0.430	3.210	6.941	1.113	0.222	3.351
17	20350	6.810	0.000	0.440	3.320	6.957	1.147	0.233	3.469
18	20357	6.610	0.000	0.410	3.010	6.738	1.136	0.201	3.142
19	20480	8.850	0.350	0.760	5.340	9.203	1.611	0.583	5.695
20	20491	7.180	0.030	0.450	3.650	7.334	1.180	0.244	3.800
21	20492	9.120	0.540	0.860	5.790	9.537	1.837	0.693	6.202
22	20527	10.900	1.260	1.280	7.530	11.587	2.707	1.152	8.221
23	20557	7.140	0.040	0.520	3.910	7.339	1.215	0.321	4.109
24	20567	6.970	0.000	0.440	3.330	7.117	1.147	0.233	3.475
25	20741	8.120	0.200	0.660	4.810	8.409	1.425	0.474	5.094
26	20762	10.440	1.040	1.150	7.220	11.043	2.441	1.010	7.826
27	20815	7.420	0.060	0.540	4.060	7.632	1.242	0.343	4.271
28	20826	7.510	0.050	0.550	4.180	7.728	1.236	0.354	4.393
29	20850	9.040	0.530	0.840	5.740	9.444	1.820	0.671	6.142
30	20899	7.850	0.130	0.610	4.510	8.107	1.337	0.419	4.770
31	20978	9.110	0.560	0.860	6.060	9.527	1.857	0.693	6.473
32	21066	7.040	0.000	0.470	3.790	7.207	1.157	0.266	3.955
33	21099	8.600	0.350	0.740	5.290	8.940	1.604	0.562	5.633
34	21112	7.770	0.060	0.540	4.180	7.982	1.242	0.343	4.387
35	21152	6.400	0.000	0.410	3.210	6.528	1.136	0.201	3.336
36	21256	10.670	1.130	1.240	7.810	11.331	2.563	1.109	8.467
37	21261	10.740	1.170	1.190	7.340	11.369	2.585	1.054	7.969
38	21267	6.620	-0.010	0.430	3.370	6.761	1.133	0.222	3.511
39	21637	7.530	0.100	0.580	4.290	7.767	1.297	0.387	4.524
40	21723	10.040	1.000	1.080	6.880	10.598	2.376	0.934	7.438
41	21788	8.830	0.240	0.700	5.120	9.144	1.480	0.518	5.430
42	22271	10.600	1.100	1.180	7.360	11.223	2.511	1.043	7.986
43	22380	8.970	0.510	0.820	5.710	9.361	1.793	0.649	6.101
44	22422	7.740	0.110	0.580	4.300	7.977	1.307	0.387	4.533
45	23069	8.890	0.350	0.740	5.310	9.230	1.604	0.562	5.649

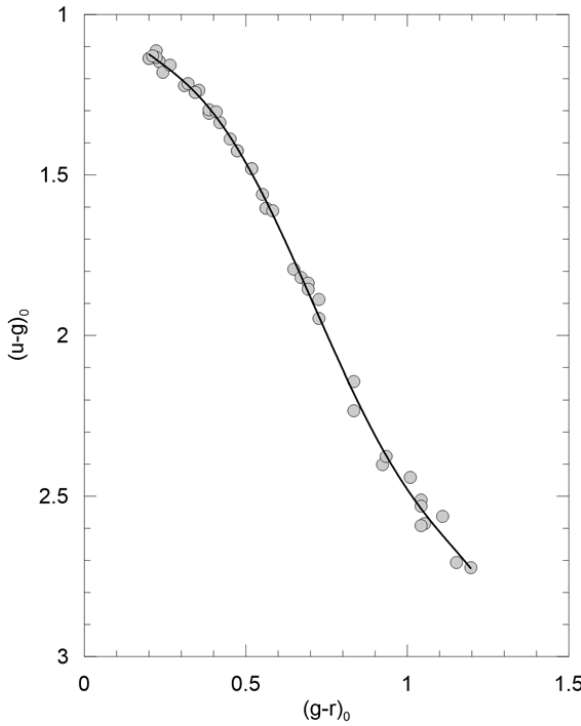


Fig. 4 The two-colour diagram of the Hyades cluster.

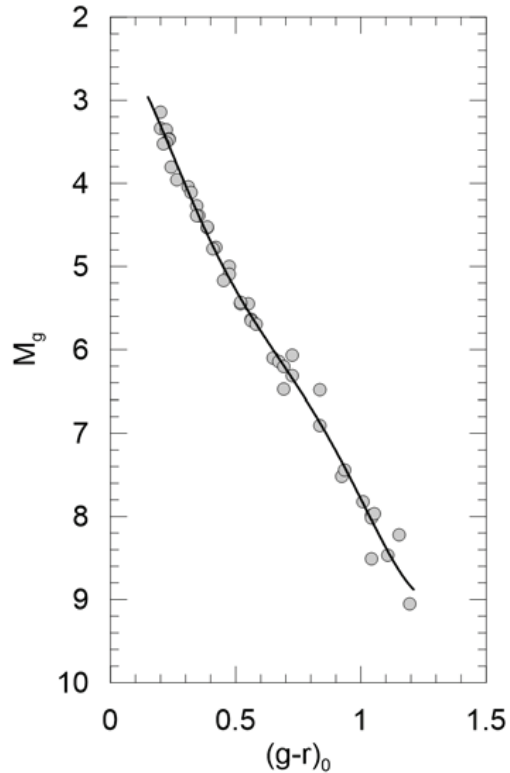


Fig. 5 The absolute magnitude-colour diagram of the Hyades cluster.

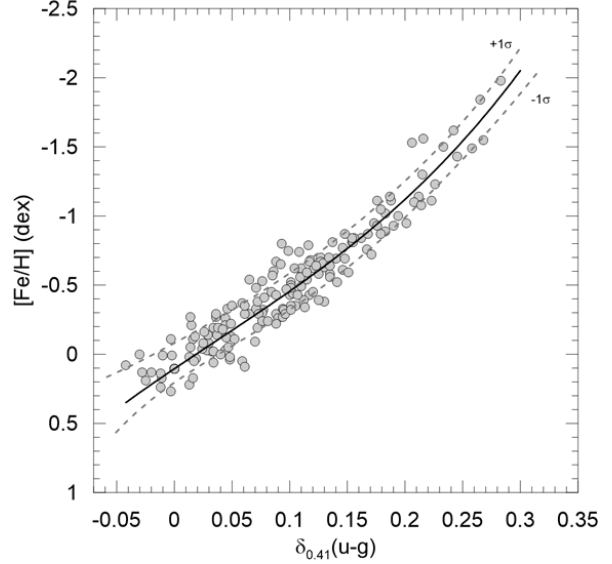


Fig. 6 Calibration of the iron abundance $[Fe/H]$ in terms of reduced UV excess, $\delta_{0.41}$. The symbol σ indicates the standard deviation estimated for the third order polynomial fitted for the calibration.

The squared correlation coefficients and the standard deviations of Eqs. (10) and (11) are $R^2 = 0.998$, $\sigma = 0.027$ and $R^2 = 0.991$, $\sigma = 0.164$, respectively. The range of the $(g-r)_0$ colour index for the Hyades cluster is $0.2 < (g-r)_0 < 1.2$ mag.

3 Procedure

3.1 Calibration of $[Fe/H]$ in terms of $\delta_{0.41}$

We used the same procedure in Paper I for metallicity calibration. We evaluated the ultra-violet excess $\delta = (u-g)_H - (u-g)_*$ for each star, where $(u-g)_*$ and $(u-g)_H$ are the de-reddened UV indices for a sample star and the Hyades star with the same $(g-r)_0$ colour index. Then, we reduced it to the UV excess corresponding to the colour index $(g-r)_0 = 0.41$ mag via the appropriate guillotine factor (f , normalized factor) in Sandage (1969), i.e. $\delta_{0.41} = f \times \delta$. Here, $(g-r)_0 = 0.41$ mag corresponds to $(B-V)_0 = 0.60$ mag in the UBV system (see also, Karaali et al. 2011). Finally, we fitted the iron abundances $[Fe/H]$ of the sample stars to a third order polynomial in terms of their reduced UV excesses, $\delta_{0.41}$ as follows (Fig. 6):

$$[Fe/H] = 0.105(0.010) - 5.633(0.521) \times \delta_{0.41} + 2.984(1.895) \times \delta_{0.41}^2 - 27.209(16.359) \times \delta_{0.41}^3. \quad (12)$$

Eq. (12) is the metallicity calibration in terms of the UV excess defined in the *ugr* system. The squared correlation coefficient and the standard deviation for our calibration are $R^2 = 0.949$ and $\sigma = 0.107$ mag, respectively. This calibration covers the stars with iron abundance $-2 < [\text{Fe}/\text{H}] < 0.3$ dex, and the range of the reduced UV excess is $-0.03 < \delta_{0.41} < 0.28$ mag.

We tested the accuracy of our calibration by calculating the iron abundances, $[\text{Fe}/\text{H}]_{\text{cal}}$, of the sample stars via replacing their reduced UV excesses, $\delta_{0.41}$, into Eq. (12) and compared them with the original ones, $[\text{Fe}/\text{H}]_{\text{org}}$. The distribution of the residuals, $\Delta[\text{Fe}/\text{H}] = [\text{Fe}/\text{H}]_{\text{org}} - [\text{Fe}/\text{H}]_{\text{cal}}$, are plotted in Fig. 7b. Their mean and the corresponding standard deviation are $\langle [\text{Fe}/\text{H}] \rangle = 0.00$ and $\sigma = 0.137$ dex, respectively. Zero mean residual and small standard deviation as well as the diagonal trend between the original and calculated iron metallicities (Fig. 7a) are indications for accuracy of our calibration.

3.2 Calibration of ΔM_g in terms of $\delta_{0.41}$

Photometric parallax estimation is based on the calibration of the absolute magnitude offset in terms of reduced UV excess. We evaluated the difference between the absolute magnitude of each sample star, $(M_g)_*$, and the corresponding Hyades star, $(M_g)_H$, with the same $(g-r)_0$ colour index as follows:

$$\Delta M_g = (M_g)_* - (M_g)_H. \quad (13)$$

Then, we fitted the ΔM_g differences to a third order polynomial in terms of the reduced UV excesses of the sample stars as follows (Fig. 8):

$$\begin{aligned} \Delta M_g = & -0.133(0.031) + 5.169(0.965) \times \delta_{0.41} \\ & -3.623(0.978) \times \delta_{0.41}^2 + 21.497(7.799) \times \delta_{0.41}^3. \end{aligned} \quad (14)$$

Eq. (14) is the absolute magnitude calibration in terms of reduced UV excess. Its squared correlation coefficient and standard deviation are $R^2 = 0.816$ and $\sigma = 0.180$ mag, respectively. The range of the reduced UV excess is $-0.03 < \delta_{0.41} < 0.30$ dex and our calibration covers the absolute magnitude residuals $-0.5 < \Delta M_g < 1.6$ mag.

We tested the accuracy of our calibration via the procedure explained in the following. We replaced the reduced UV excesses of the sample stars into Eq. (14) and evaluated the absolute magnitude offsets, $(\Delta M_g)_{\text{cal}}$, of the sample stars. Then, we adopted Eq. (13) and evaluated an absolute magnitude for each sample star:

$$(M_g)_{\text{cal}} = (M_g)_H + (\Delta M_g)_{\text{cal}}. \quad (15)$$

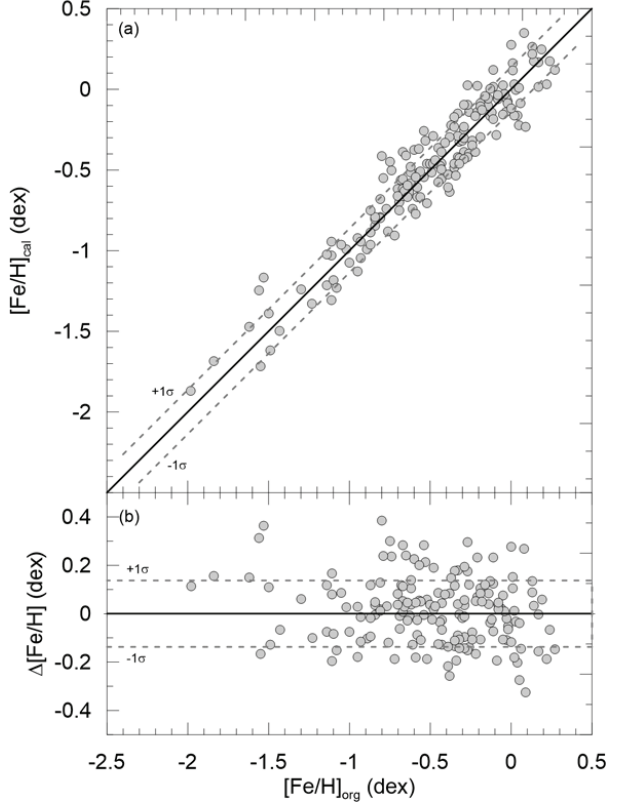


Fig. 7 The relation between the original iron abundances and the estimated ones (panel a), and the distribution of the residuals relative to the original iron abundances (panel b). The symbol σ is the same as in Fig. 6.

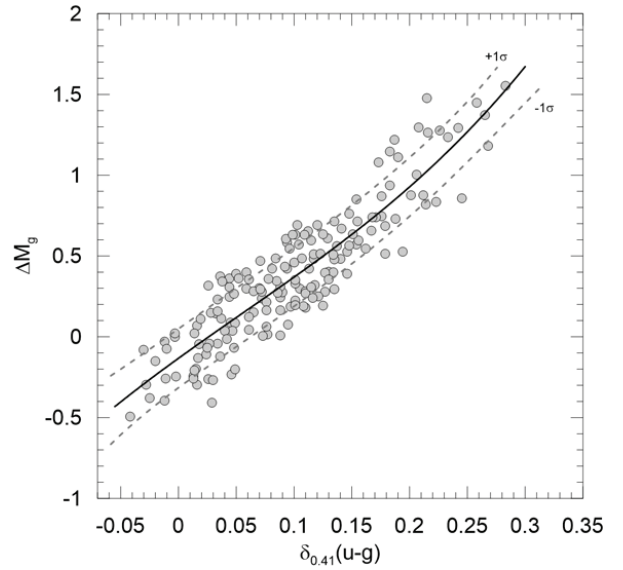


Fig. 8 Diagram for the absolute magnitude offset, ΔM_g , versus UV excess, $\delta_{0.41}$. The symbol σ is the same as in Fig. 6.

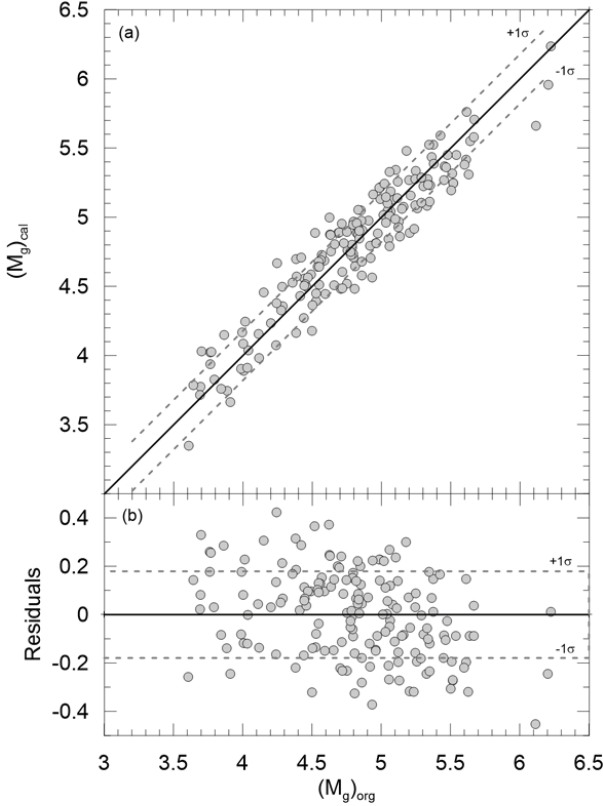


Fig. 9 The relation between the original absolute magnitudes and the estimated ones (panel a), and the distribution of the residuals relative to the original absolute magnitudes (panel b). The symbol σ is the same as in Fig. 6.

Here, $(M_g)_H$ is the absolute magnitude of the Hyades star with the same $(g - r)_0$ of the star in question. The $(M_g)_{\text{cal}}$ absolute magnitudes are tabulated in the seventh column of Table 3. Finally, we estimated the absolute magnitude residuals, the differences between the original and evaluated absolute magnitudes:

$$\text{Residuals} = (M_g)_{\text{org}} - (M_g)_{\text{cal}}. \quad (16)$$

The mean of the residuals ($\langle \text{Res} \rangle$) and the corresponding standard deviation (σ) are 0 and 0.179 mag, respectively. The evaluated absolute magnitudes and the residuals are plotted in Fig. 9. As in the case of metallicity calibration, zero mean residual, relatively small standard deviation and diagonal trend in the distribution of evaluated versus original absolute magnitudes is an indication for the accuracy of our absolute magnitude calibration.

4 Application of the Procedure

We estimated vertical metallicity gradients by applying our metallicity calibration to a sample of stars in a

high Galactic latitude field with a series of constraints as explained in the following. Metallicity gradients can be estimated in the vertical or radial directions for the objects in our Galaxy. It has been shown that there are large numerical differences between two kind of metallicity gradients. Also, any one of these metallicity gradients (vertical or radial) is depends on many parameters such as population type, the Galactic coordinates and distance range of the objects for which the metallicity gradient is carried out (cf. Önal Taş et al. 2016). Here, our data consist of dwarfs. Hence we tabulated the vertical metallicity gradients for the dwarfs appeared in the literature in Table 4 for comparison purpose. Thus, we applied the following constraints to a star sample and estimated the vertical metallicity gradients: *i*) Galactic coordinates and size: $85^\circ \leq b \leq 90^\circ$, $0^\circ \leq l \leq 360^\circ$; $A=78 \text{ deg}^2$, *ii*) Luminosity class: F-G dwarfs, and *iii*) Absolute magnitude $4 < M_g \leq 6$ mag.

4.1 The star sample

The data for the application of the procedure are provided from the recent survey DR 12 of SDSS III (Alam et al. 2015). There are 1,973,575 objects with de-reddened $ugriz$ magnitudes in the star field defined above. The SDSS magnitudes and their errors are supplied from SQL webpage of SDSS¹. Following Chen et al. (2001), we restricted our data with $g_o \leq 23$ and $(u - g)_o > 0.5$ mag to avoid from the extra galactic objects. Then our sample reduced to 433,636. One sees in Fig. 10 a large scattering of these stars in the $(g - r)_0 \times (r - i)_0$ two-colour diagram. We adopted the following equation of Juric et al. (2008) and limited the number of stars as 411,512 which are within $\pm 2\sigma$ of this equation:

$$(g - r)_0 = 1.39(1 - \exp[-4.9(r - i)_0^3 - 2.45(r - i)_0^2 - 1.68(r - i)_0 - 0.050]). \quad (17)$$

Finally, we used the following equations of Helmi et al. (2003) (see also, Bilir et al. 2008c) and identified 131 giants from the sample:

$$\begin{aligned} 1.1 &\leq (u - g)_0 \leq 2, \\ -0.1 &< P_1 < 0.6, \\ |s| &> m_s + 0.05. \end{aligned} \quad (18)$$

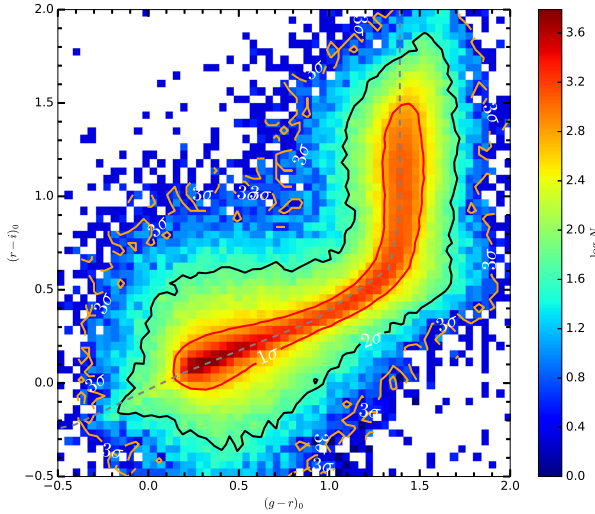
¹<https://skyscraper.sdss.org/dr12/en/tools/search/sql.aspx>

Table 3 Apparent and absolute magnitudes for 168 sample stars used in the calibrations. The columns give: ID, Hipparcos number, trigonometric parallax (π), apparent magnitude (g_0), original absolute magnitude ($(M_g)_{org}$), absolute magnitude offset (ΔM_g), estimated absolute magnitude ($(M_g)_{cal}$) and the residuals.

ID	Hip	π (mas)	g_0 (mag)	$(M_g)_{org}$ (mag)	ΔM_g (mag)	$(M_g)_{cal}$ (mag)	Residual (mag)	ID	Hip	π (mas)	g_0 (mag)	$(M_g)_{org}$ (mag)	ΔM_g (mag)	$(M_g)_{cal}$ (mag)	Residual (mag)
1	493	26.93	7.656	4.807	0.375	4.482	-0.325	85	57017	18.78	7.670	4.038	0.310	4.037	-0.001
2	910	53.34	5.065	3.700	-0.231	4.030	0.330	86	57265	6.25	10.480	4.459	0.745	4.496	0.037
3	1599	116.46	4.457	4.788	0.237	4.780	-0.008	87	57443	108.45	5.169	5.345	0.196	5.523	0.178
4	1976	21.27	7.805	4.444	-0.379	4.558	0.114	88	57450	12.85	10.123	5.668	1.236	5.579	-0.089
5	2711	39.24	5.726	3.695	-0.041	3.776	0.081	89	58843	14.24	9.431	5.199	0.596	5.270	0.071
6	3182	16.76	8.963	5.084	0.153	5.125	0.041	90	58950	27.85	8.034	5.258	0.233	5.065	-0.193
7	3479	30.89	8.068	5.517	0.362	5.244	-0.273	91	59380	27.31	7.723	4.905	0.480	4.977	0.072
8	3497	45.34	6.822	5.104	0.016	5.341	0.237	92	61053	45.92	6.408	4.718	0.360	4.487	-0.231
9	3704	20.51	8.028	4.588	0.298	4.685	0.097	93	61619	17.81	7.509	3.762	-0.068	3.939	0.177
10	3909	63.48	5.368	4.381	0.308	4.162	-0.219	94	62108	8.17	9.989	4.550	1.003	4.513	-0.037
11	4544	9.23	9.811	4.637	0.685	4.752	0.115	95	62207	57.55	6.161	4.961	0.596	4.811	-0.150
12	4892	16.48	8.735	4.820	0.243	4.886	0.066	96	62809	20.67	8.672	5.249	0.525	5.336	0.087
13	5163	10.84	9.656	4.831	0.189	5.052	0.221	97	64345	16.88	8.977	5.114	0.273	5.140	0.026
14	5301	18.23	8.655	4.959	-0.002	4.813	-0.146	98	64394	109.54	4.459	4.657	0.112	4.509	-0.148
15	5862	66.16	5.185	4.288	-0.257	4.355	0.067	99	64698	18.48	8.709	5.043	-0.045	5.047	0.004
16	6159	15.35	9.101	5.032	0.397	5.144	0.112	100	64747	21.87	8.545	5.244	0.248	5.085	-0.159
17	7217	14.60	9.209	5.031	0.295	4.960	-0.071	101	65418	3.12	12.281	4.752	1.263	4.520	-0.232
18	7459	10.87	10.269	5.450	1.278	5.270	-0.180	102	66238	33.27	7.571	5.181	0.009	5.481	0.300
19	7978	57.36	5.734	4.527	0.299	4.392	-0.135	103	67655	39.42	8.225	6.204	1.111	5.959	-0.245
20	8859	24.12	6.880	3.792	0.216	3.824	0.032	104	67863	16.70	9.250	5.364	0.659	5.434	0.070
21	9085	37.22	6.259	4.113	0.276	4.156	0.043	105	68030	40.22	6.336	4.358	0.356	4.527	0.169
22	10449	15.87	9.287	5.290	0.739	5.286	-0.004	106	70319	58.17	6.514	5.337	0.359	5.236	-0.101
23	10652	15.93	9.199	5.210	0.511	5.156	-0.054	107	70681	21.04	9.498	6.113	1.478	5.660	-0.453
24	12294	5.82	10.619	4.444	0.875	4.503	0.059	108	70829	19.18	9.200	5.614	0.399	5.761	0.147
25	12306	29.17	7.536	4.861	0.329	4.906	0.045	109	71076	17.24	7.969	4.152	0.193	4.458	0.306
26	12444	45.96	5.963	4.275	0.124	4.325	0.050	110	71735	37.71	7.635	5.517	0.390	5.246	-0.271
27	12653	58.25	5.614	4.440	0.021	4.271	-0.169	111	72407	10.65	10.011	5.148	0.282	5.060	-0.088
28	12777	89.87	4.264	4.032	0.159	3.913	-0.119	112	72673	20.06	7.259	3.771	0.296	4.027	0.256
29	12889	20.16	7.860	4.382	-0.202	4.698	0.316	113	74067	26.62	8.206	5.332	0.716	5.277	-0.055
30	13366	16.39	8.419	4.492	0.483	4.588	0.096	114	75181	67.51	5.912	5.059	0.075	5.328	0.269
31	14241	28.54	8.335	5.612	0.485	5.416	-0.196	115	78640	8.41	10.000	4.624	0.859	4.997	0.373
32	15131	41.34	6.983	5.065	0.481	5.041	-0.024	116	81520	44.54	7.258	5.502	0.691	5.196	-0.306
33	15158	10.55	8.647	3.763	-0.261	4.023	0.260	117	81681	33.82	7.413	5.059	0.279	5.009	-0.050
34	15381	20.16	7.721	4.243	-0.493	4.378	0.135	118	83229	32.77	7.217	4.794	0.269	4.946	0.152
35	16169	21.38	8.468	5.118	0.283	5.256	0.138	119	83489	13.43	9.351	4.991	0.007	5.218	0.227
36	17147	39.12	6.871	4.833	0.571	4.918	0.085	120	84988	35.67	7.223	4.985	0.280	5.214	0.229
37	22632	15.00	9.280	5.160	1.294	5.077	-0.083	121	85007	34.12	7.040	4.705	0.653	4.483	-0.222
38	23555	31.50	6.500	3.992	-0.243	4.169	0.177	122	85042	51.22	6.505	5.052	-0.081	4.841	-0.211
39	23688	8.79	9.779	4.499	1.146	4.177	-0.322	123	86013	19.38	8.576	5.013	0.561	5.015	0.002
40	24030	8.66	9.832	4.520	0.525	4.886	0.366	124	86321	8.38	9.888	4.504	0.761	4.365	-0.139
41	25860	20.07	8.774	5.287	0.356	5.105	-0.182	125	87062	9.59	10.442	5.351	1.449	5.231	-0.120
42	26617	8.79	10.337	5.057	0.632	4.789	-0.268	126	88945	40.29	7.098	5.124	0.265	4.968	-0.156
43	27072	112.02	3.760	4.006	0.147	3.889	-0.117	127	92270	34.78	6.280	3.987	0.020	3.906	-0.081
44	28403	19.64	8.838	5.304	0.420	5.223	-0.081	128	92532	32.72	7.347	4.921	0.631	4.705	-0.216
45	28671	16.81	9.511	5.639	0.871	5.550	-0.089	129	92781	14.59	9.225	5.045	0.566	5.101	0.056
46	29432	42.55	7.092	5.236	0.317	4.918	-0.318	130	93185	41.94	7.009	5.122	0.545	4.926	-0.196
47	31188	16.79	8.716	4.841	0.634	4.846	0.005	131	94129	17.60	8.432	4.660	-0.206	4.805	0.145
48	33582	12.56	9.217	4.712	0.180	4.953	0.241	132	94645	36.30	6.439	4.239	-0.030	4.074	-0.165
49	34017	52.27	6.163	4.754	0.087	4.761	0.007	133	96124	36.72	7.420	5.245	0.084	5.275	0.030
50	34511	21.64	8.240	4.916	0.069	4.796	-0.120	134	96258	39.82	5.884	3.885	0.149	3.745	-0.140
51	35139	30.95	8.002	5.455	0.669	5.370	-0.085	135	98355	19.11	7.610	4.016	0.251	4.243	0.227
52	36491	20.20	8.677	5.204	1.081	4.887	-0.317	136	99139	17.95	9.078	5.348	0.399	5.113	-0.235
53	36849	12.37	9.109	4.571	0.547	4.725	0.154	137	99938	17.64	8.588	4.820	0.308	4.958	0.138
54	37419	19.16	8.915	5.327	0.468	5.083	-0.244	138	100017	56.92	6.083	4.859	0.341	4.578	-0.281
55	38541	34.30	8.548	6.224	1.371	6.236	0.012	139	100279	10.46	10.278	5.376	0.741	5.388	0.012
56	38769	11.56	8.969	4.284	0.239	4.497	0.213	140	100568	22.78	8.840	5.628	1.297	5.310	-0.318
57	40118	45.90	7.116	5.425	0.188	5.591	0.166	141	100792	17.00	8.478	4.630	0.836	4.872	0.242
58	40778	10.35	9.864	4.939	1.182	5.163	0.224	142	102018	24.89	7.433	4.413	-0.298	4.430	0.017
59	41484	44.94	6.577	4.840	-0.068	4.902	0.062	143	102046	16.15	8.381	4.422	0.513	4.709	0.287
60	42356	22.91	7.827	4.627	-0.298	4.874	0.247	144	102762	17.11	8.304	4.470	-0.107	4.566	0.096
61	43595	7.87	11.031	5.511	0.850	5.317	-0.194	145	102805	32.66	6.121	3.691	0.352	3.713	0.022
62	43726	57.52	6.299	5.098	-0.074	4.987	-0.111	146	103458	45.17	6.746	5.020	0.391	5.241	0.221
63	44116	12.70	8.598	4.117	0.635	3.981	-0.136	147	103498	18.95	8.466	4.854	0.731	4.977	0.123
64	44713	26.83	7.544	4.687	-0.395	4.887	0.200	148	103897	7.70	10.318	4.750	0.166	4.893	0.143
65	44811	24.53	7.829	4.777	0.515	4.750	-0.027	149	104659	29.10	7.530	4.849	0.818	5.049	0.200
66	47048	10.26	8.551	3.607	0.632	3.349	-0.258	150	107294	9.03	10.155	4.933	1.219	4.562	-0.371
67	47174	11.99	10.205	5.599	0.691	5.380	-0.219	1							

Table 4 Vertical metallicity gradients appeared in the literature for the dwarf stars. Z in kpc.

Authors	$d[\text{Fe}/\text{H}]/dZ$ (dex kpc^{-1})	Region	Remark	Survey
Mikolaitis et al. (2014)	-0.107 ± 0.009	Solar neighbourhood	$0 < Z < 4.50$	Gaia-ESO
	-0.072 ± 0.006	Solar neighbourhood	$0 < Z < 4.25$	Gaia-ESO
Schlesinger et al. (2014)	-0.257	$b > 10^\circ$	$0.27 \leq Z \leq 1.62$	SDSS-SEGUE
Peng et al. (2012)	-0.160 ± 0.060	$55^\circ \leq l \leq 260^\circ, 35^\circ \leq b \leq 70^\circ$	$2 < Z < 5$	BATC & SDSS
Kordopatis et al. (2011)	-0.140 ± 0.050	$l \sim 277^\circ, b \sim 47^\circ$	$1 \leq Z \leq 4$	ESO
Yaz & Karaali (2010)	-0.320 ± 0.010	$0^\circ \leq l \leq 100^\circ, 140^\circ \leq l \leq 160^\circ, \langle b \rangle = 45^\circ$	$Z < 2.5$	SDSS
Ak et al. (2007a)	-0.380 ± 0.060	$0^\circ \leq l \leq 360^\circ, 60^\circ \leq b \leq 65^\circ$	$3 \leq Z < 5$	SDSS
Ak et al. (2007b)	-0.160 ± 0.020	$(l, b) = (180^\circ, 45^\circ)$	$Z < 3$	SDSS
Karaali et al. (2003b)	-0.20	$(l, b) = (52^\circ, -39^\circ)$	$Z \leq 8$	Deep Multicolor
Bartašiūtė et al. (2003)	-0.230 ± 0.040	$0^\circ \leq l \leq 100^\circ, 59^\circ \leq b \leq 76^\circ$	$Z < 1.3$	Vilnius

**Fig. 10** $(g-r)_0 \times (r-i)_0$ two-colour diagram for 433,636 stars. The dotted mean line corresponds to the equation of Juric et al. (2008), while the lines with red, black and orange colours cover the stars within 1σ , 2σ and 3σ of the mean line, respectively.

where P_1 , s and m_s are defined as follows:

$$\begin{aligned} P_1 &= 0.910(u-g)_0 + 0.415(g-r)_0 - 1.28, \\ s &= -0.249u_0 + 0.794g_0 - 0.555r_0 + 0.240, \\ m_s &= 0.12. \end{aligned} \quad (19)$$

The position of giants are shown in the $(u-g)_0 \times (g-r)_0$ and $(g-r)_0 \times (r-i)_0$ two-colour diagrams of Fig. 11. Thus, our sample reduced to 411,381 dwarfs.

We considered the errors of dwarfs in the final sample and omitted the ones with large errors from the sample to obtain more accurate results, as explained in the following. Fig. 12 shows that the errors for g magnitudes and, $g-r$ and $u-g$ colours are small for a large range of g_0 apparent magnitude, while they increase up to 0.25, 0.35 and 1.5 mag, respectively, with increasing g_0 . Hence, we restricted the faint limit of the de-reddened apparent magnitude with $g_0 = 20$ mag to avoid from large errors in magnitude and colours. Thus, the median errors for g_0 , $(g-r)_0$, and $(u-g)_0$ for the sample

of dwarfs with $14 < g_0 \leq 20$ ($N=27,304$) are 0.03, 0.04 and 0.11 mag, respectively.

Our final constraint is related to the absolute magnitudes of the stars which are estimated via the procedure in Section 3. We considered only the dwarf stars whose absolute M_g magnitudes are defined in our calibrations, i.e. $4 < M_g \leq 6$ mag. Thus, the application of the metallicity calibration will be carried out for 23,414 dwarf stars.

4.2 Vertical metallicity gradient

We estimated vertical metallicity gradients for three sub-samples with different absolute magnitudes, i.e. $4 < M_g \leq 6$, $4 < M_g \leq 5$ and $5 < M_g \leq 6$ mag. The number of stars in these sub-samples are 23,414, 6,833 and 16,581, respectively. The distances of the stars are evaluated by the Pogson formula and they are reduced to the vertical distances (Z) by the equation $Z = r \sin(b)$, where r and b are the distance to a star relative to the Sun and its Galactic latitude, respectively. The distance error of a star is mainly comes

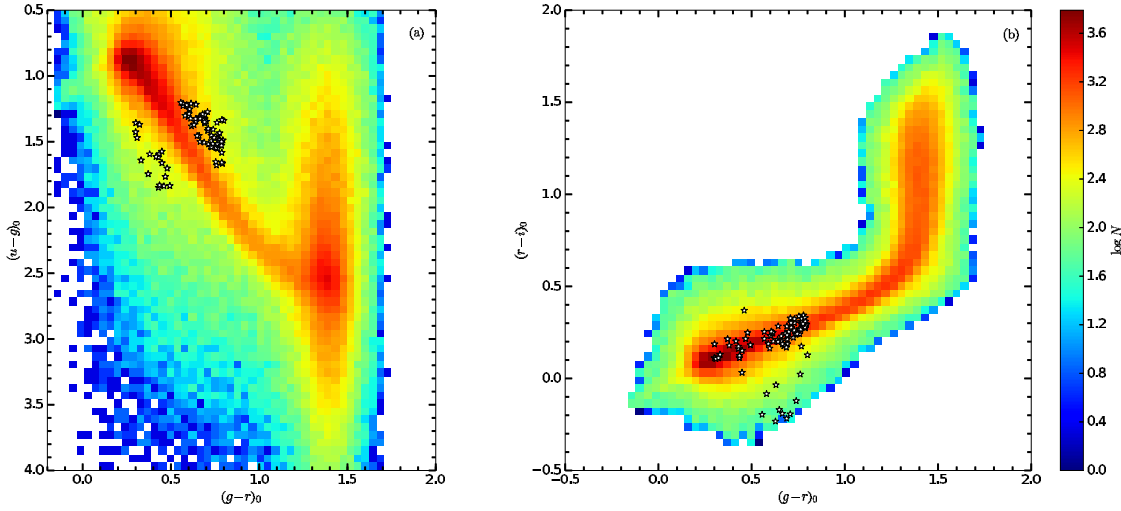


Fig. 11 $(u - g)_0 \times (g - r)_0$ and $(g - r)_0 \times (r - i)_0$ two-colour diagrams for 411,512 stars within 2σ of the mean line. 131 giant stars are marked with black star symbol in the diagrams.

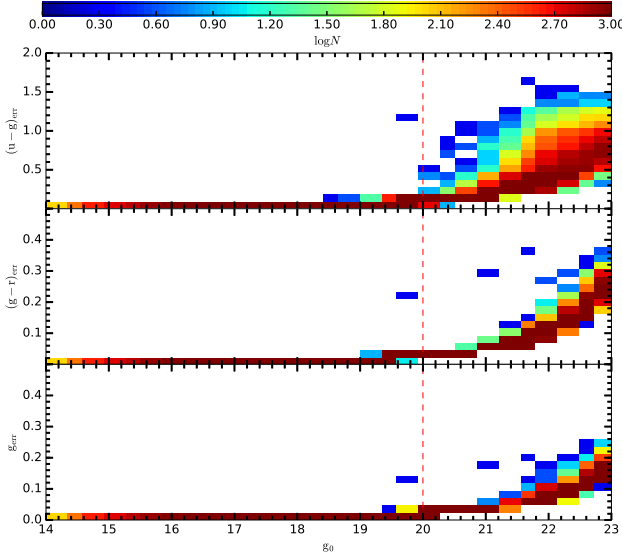


Fig. 12 Error distributions for the apparent magnitude g and colours $u - g$ and $g - r$ as a function of apparent g_0 magnitude.

from its apparent and absolute magnitudes. The rms error of the absolute magnitude in our new distance calibration is 0.18 mag (see, Eq. 14). As seen in Fig. 12, the median magnitude error for the apparent magnitude $g_0 = 20$ becomes 0.03 mag. Thus, the errors in the distance modules of the stars in our study do not exceed 0.185 mag. This maximum magnitude error in the distance module corresponds to the distance errors of about 180, 450 and 900 pc at 2, 5 and 10 kpc.

The distribution of the metallicities for three subsamples are demonstrated in Fig. 13a-c and the evaluated metallicity gradients for the distance intervals $0 < Z \leq 5$, $0 < Z \leq 2$, $2 < Z \leq 5$ and $Z > 5$ kpc are listed in Table 5. The metallicity gradients are deep for the stars with $0 < Z \leq 5$, $0 < Z \leq 2$, $2 < Z \leq 5$ kpc in three absolute magnitude intervals, $4 < M_g \leq 6$, $4 < M_g \leq 5$ and $5 < M_g \leq 6$ mag. While they are all positive numbers, such as $d[\text{Fe/H}]/dZ = +0.046 \pm 0.008$ dex kpc $^{-1}$ for the stars with absolute magnitude $4 < M_g \leq 5$, beyond $Z = 5$ kpc. The vertical metallicity gradients appeared in the literature are deepest at small Z distances. Whereas, Table 5 and Fig. 13a-c show that the deepest metallicity gradient can occur at larger Z distances. For instance, the deepest metallicity gradient, $d[\text{Fe/H}]/dZ = -0.202 \pm 0.029$ dex kpc $^{-1}$ in the absolute magnitude interval $4 < M_g \leq 6$ mag belongs to stars with small vertical distances, $0 < Z \leq 2$ kpc, agreeable with the results in the literature. Whereas, the deepest metallicity gradients in the absolute magnitude intervals $4 < M_g \leq 5$ and $5 < M_g \leq 6$ mag, i.e. $d[\text{Fe/H}]/dZ = -0.324 \pm 0.026$ and $d[\text{Fe/H}]/dZ = -0.187 \pm 0.013$ dex kpc $^{-1}$ respectively, are the ones for stars with larger vertical distances, $2 < Z \leq 5$ kpc.

As stated in the previous paragraph, vertical metallicity gradients appeared in the literature are deep at small vertical distances, while they are less deep or flat at large Z distances. Small Z distances cover the Galactic region dominated by the thin-disc population, whereas thick-disc stars are significant at larger vertical distances. Here, we showed that metallicity gradients

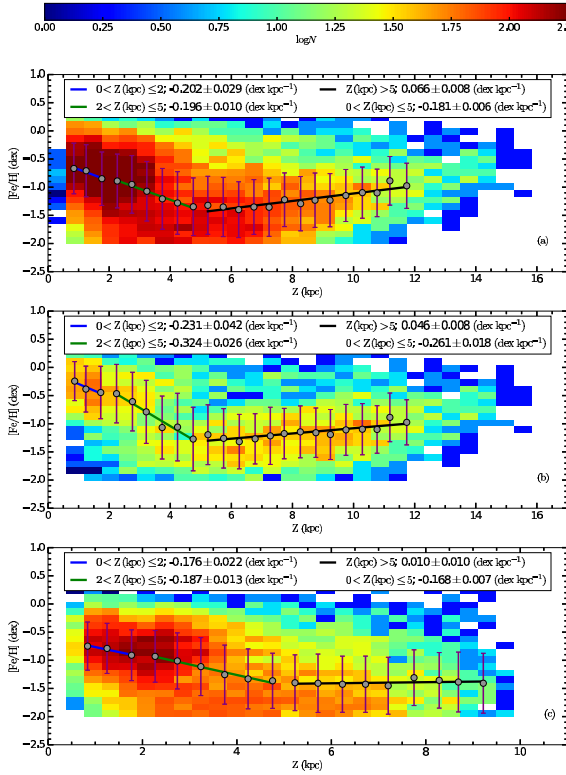


Fig. 13 Distributions of the [Fe/H] in terms of vertical distance Z in three panels: for dwarf stars with (a) $4 < M_g \leq 6$, (b) for $4 < M_g \leq 5$ and (c) for $5 < M_g \leq 6$ mag.

are also absolute magnitude dependent. Actually, the vertical distance intervals of the stars with the deepest metallicity gradients in different absolute magnitude intervals are different. In the following section, we will investigate the relation between our finding and the ones already appeared in the literature.

4.3 Identification of the metallicity gradient in term of absolute magnitude and population type

We plotted the histogram for the stars with $4 < M_g \leq 6$ mag for interpretation of our results. Fig. 14 shows that the distribution is bimodal, indicating two different star categories. Actually, it could be dissolved into

Table 5 Vertical metallicity gradients, $d[\text{Fe}/\text{H}]/dZ$ (dex kpc^{-1}), as a function of vertical distance Z (kpc) and absolute magnitude M_g (mag) estimated in this study.

Z (kpc)	$4 < M_g \leq 6$ $d[\text{Fe}/\text{H}]/dZ$	$4 < M_g \leq 5$ $d[\text{Fe}/\text{H}]/dZ$	$5 < M_g \leq 6$ $d[\text{Fe}/\text{H}]/dZ$
$0 < Z \leq 5$	-0.181 ± 0.006	-0.261 ± 0.018	-0.168 ± 0.007
$0 < Z \leq 2$	-0.202 ± 0.029	-0.231 ± 0.042	-0.176 ± 0.022
$2 < Z \leq 5$	-0.196 ± 0.010	-0.324 ± 0.026	-0.187 ± 0.013
$Z > 5$	$+0.066 \pm 0.008$	$+0.046 \pm 0.008$	$+0.010 \pm 0.010$

two different histograms with single modes by overlapping of the histograms for the stars with $4 < M_g \leq 5$ and $5 < M_g \leq 6$ mag on the same diagram. The mode for the bright absolute magnitudes correspond to $(g-r)_0 \approx 0.22$ mag, while for fainter ones it is at $(g-r)_0 \approx 0.38$ mag. We separated the sample stars into two apparent magnitude intervals, $g_0 \leq 18$ and $g_0 > 18$ mag, and repeated our procedure to obtain a detailed result. For apparently bright stars in the panel (a) of Fig. 15, the mode for the stars with absolute magnitudes $5 < M_g \leq 6$ almost kept its position in Fig. 14, while the other one moved from $(g-r)_0 \approx 0.22$ mag to $(g-r)_0 \approx 0.35$ mag. Contrary to the diagram in the panel (a), bimodal structure for stars with $4 < M_g \leq 6$ mag in the panel (b) for apparently faint stars is more evident. One can observe a slight shift of the mode for stars with $5 < M_g \leq 6$ mag, relative to the one in Fig. 14. While, the mode for the stars with $4 < M_g \leq 5$ mag is now at a position rather different than the one in panel (a), but almost equal to the one in Fig. 14, i.e. $(g-r)_0 \approx 0.22$ mag.

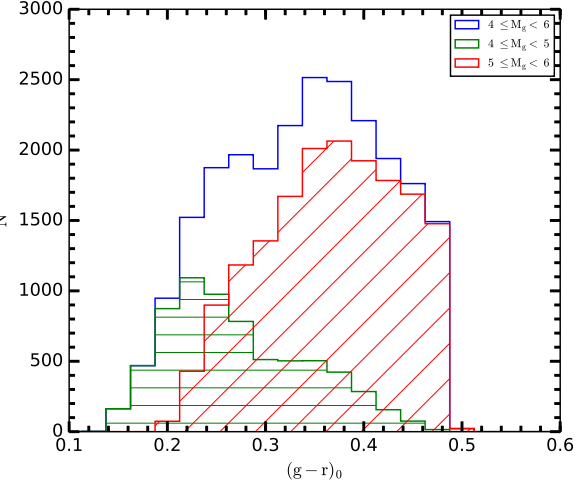


Fig. 14 Histograms for dwarf stars with absolute magnitudes $4 < M_g \leq 6$, $4 < M_g \leq 5$ and for $5 < M_g \leq 6$ mag.

Chen et al. (2001) investigated the distribution of stars in the $g_0 \times (g-r)_0$ colour magnitude diagram for two large samples north and south of the Galactic plane and revealed the positions of three different populations, i.e. thin disc, thick disc and halo. In their Fig. 6, one sees a gross bimodal structure in $(g-r)_0$, reflecting the separation of halo/thick disc at $(g-r)_0 \approx 0.3$ mag and the thin-disc population at $(g-r)_0 \approx 1.3$ mag. Our histogram in Fig. 14 is also bimodal and the mode at the blue side is a bit left of $(g-r)_0 \approx 0.3$ mag, while their mode at $(g-r)_0 \approx 1.3$ mag does not appear in

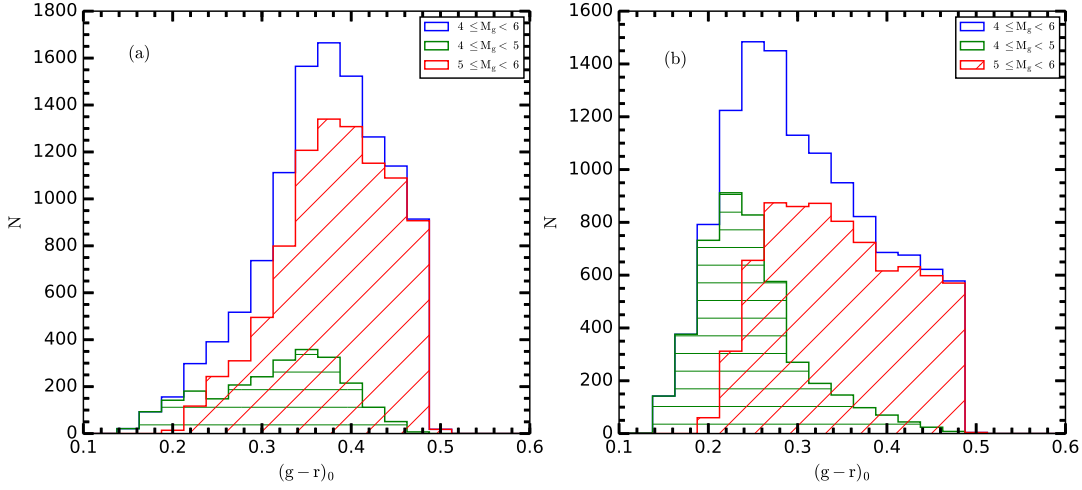


Fig. 15 The same as in Fig. 14, but for two different apparent magnitudes: (a) for $g_0 \leq 18$ and (b) for $g_0 > 18$ mag.

our Fig. 14, due to our restrictions. However, there exist a second mode at $(g-r)_0 \approx 0.38$ mag. Chen et al. (2001) showed also that in the range $15 < g_0 < 18$ mag, the blue stars are dominated by thick-disc stars with a turnoff of $(g-r)_0 \approx 0.33$ mag, a value rather close to the colour of the mode of the histogram for the stars with $4 < M_g \leq 5$ mag in Fig. 15a, i.e. $(g-r)_0 \approx 0.35$ mag. Then, one can say that stars with apparent magnitude $g_0 < 18$ and absolute magnitude $4 < M_g \leq 5$ are dominated by thick-disc stars. In the Fig. 6 of Chen et al. (2001), for $g_0 > 18$ mag the Galactic halo, which has a turnoff colour $(g-r)_0 \approx 0.2$ mag, becomes significant. This colour is rather close to the one of the mode of the histogram for stars with $g_0 > 18$ mag and absolute magnitudes $4 < M_g \leq 5$ in Fig. 15b, $(g-r)_0 \approx 0.22$ mag. Then, we can say that stars with apparent magnitude $g_0 > 18$ and absolute magnitude $4 < M_g \leq 5$ are dominated by halo stars. It seems that the modes at colours $(g-r)_0 \approx 0.38$ mag in both panels of Fig. 15 correspond to thin-disc stars. Then, we can consider the stars with any apparent magnitude but with absolute magnitudes $5 < M_g \leq 6$ as thin-disc stars. We should add that additional stars with absolute magnitudes fainter than $M_g = 6$ mag may shift the colour of the mode of the thin-disc stars up to $(g-r)_0 \approx 1.3$ mag, as in Chen et al. (2001).

In summary, significant number of stars with absolute magnitude $5 < M_g \leq 6$ belong to the thin disc population. Whereas, thick disc and halo stars share the absolute magnitude $4 < M_g \leq 5$, i.e. stars with apparent magnitude $g_0 < 18$ are thick disc stars, while apparently faint ones are dominated by the halo population. Now, if we turn back to Table 5 in our study, we see that the deep metallicity gradient -0.324 ± 0.026

dex kpc $^{-1}$ estimated for the stars with absolute magnitudes $4 < M_g \leq 5$, and vertical distances $2 < Z \leq 5$ kpc corresponds to the thick disc population. While the flat one for stars with the same absolute magnitudes but for vertical distances $Z > 5$ kpc (hence for apparently fainter stars), $d[\text{Fe}/\text{H}]/dZ = +0.046 \pm 0.008$ dex kpc $^{-1}$, is a typical value for the halo population.

Two metallicity gradients for stars with absolute magnitudes $5 < M_g \leq 6$, $d[\text{Fe}/\text{H}]/dZ = -0.176 \pm 0.022$ and $d[\text{Fe}/\text{H}]/dZ = -0.187 \pm 0.013$ dex kpc $^{-1}$, for the consecutive vertical distance intervals $0 < Z \leq 2$ and $2 < Z \leq 2$ kpc are close the each other. Then one can say that the thin disc stars which dominate the cited absolute magnitude intervals occupy a large region in the vertical direction of our Galaxy with an intermediate vertical metallicity gradient.

5 Summary and Discussion

We calibrated the [Fe/H] abundances and ΔM_g absolute magnitude offsets of a sample of 168 F-G type dwarf stars in terms of reduced UV excess, $\delta_{0.41}$, defined with the *ugr* data in SDSS. The iron abundances used in our calibrations are the updated ones used in Paper I (originally taken from Bensby et al. 2014; Nissen & Schuster 2010; Reddy et al. 2006; Venn et al. 2004). The *ugr* data of the sample stars are transformed from their *UBV* data. The distances are evaluated by using the re-reduced trigonometric parallaxes (van Leeuwen 2007) and the M_g absolute magnitudes are evaluated by the Pogson equation. The procedures used in the calibrations of [Fe/H] and ΔM_g are the same as the corresponding ones in Paper I, i.e. each of the

$[\text{Fe}/\text{H}]$ and ΔM_g are fitted to a third order polynomial in terms of $\delta_{0.41}$. The corresponding squared correlation coefficients and standard deviations are $R^2 = 0.949$, $\sigma = 0.107$ mag; and $R^2 = 0.816$, $\sigma = 0.180$ mag, respectively.

We applied the metallicity calibration to a set of stars in a high latitude Galactic field with size 78 deg^2 , i.e. $85^\circ \leq b \leq 90^\circ$, $0^\circ \leq l \leq 360^\circ$. Our calibrations are restricted with absolute magnitudes $4 < M_g \leq 6$. Hence we considered only the stars, totally $N = 23,414$, which supply our restriction in absolute magnitude. Also, we limited the apparent magnitudes of the stars (dwarfs) with $14 < g_0 \leq 20$ mag to avoid from large magnitude and colour errors.

We estimated metallicity gradients as a function of vertical distance, $0 < Z \leq 5$, $0 < Z \leq 2$, $2 < Z \leq 5$, $Z > 5$ kpc, for stars with absolute magnitude, $4 < M_g \leq 6$, $4 < M_g \leq 5$ and $5 < M_g \leq 6$. Some of our results (Table 5, Fig. 13) confirm the ones in the literature, however some of them need explanation. Vertical metallicity gradients for dwarfs with $Z > 5$ kpc in our study are all positive numbers for all absolute magnitude intervals, agreeable with the expectation that the vertical metallicity gradient is not deep at large Z distances. Also, in the absolute magnitude interval $4 < M_g \leq 6$, the gradient $d[\text{Fe}/\text{H}]/dZ = -0.202 \pm 0.029 \text{ dex kpc}^{-1}$ for $0 < Z \leq 2$ kpc is deeper than the one for larger Z distances, $2 < Z \leq 5$, i.e. $d[\text{Fe}/\text{H}]/dZ = -0.196 \pm 0.010 \text{ dex kpc}^{-1}$, again agreeable with the findings appeared in the literature. Whereas, the case is different for $d[\text{Fe}/\text{H}]/dZ = -0.231 \pm 0.042$ and $d[\text{Fe}/\text{H}]/dZ = -0.324 \pm 0.026 \text{ dex kpc}^{-1}$ in the absolute magnitude interval $4 < M_g \leq 5$, in the sense that the deeper gradient corresponds to larger Z distances, $2 < Z \leq 5$ kpc. This is new and it needs explanation. In Section 4, we showed that thick disc and halo stars share the absolute magnitudes $4 < M_g \leq 5$. It seems that the thick-disc stars dominate the vertical distance interval $2 < Z \leq 5$ kpc with a gradient of $d[\text{Fe}/\text{H}]/dZ = -0.324 \pm 0.026 \text{ dex kpc}^{-1}$, while the halo stars which are apparently fainter ($g_0 > 18$ mag) are significant at larger Z distances with gradient $d[\text{Fe}/\text{H}]/dZ = +0.046 \pm 0.008 \text{ dex kpc}^{-1}$ (Table 5 and Fig. 13b). As we stated in Section 4, the absolute magnitudes $5 < M_g \leq 6$ are dominated with the thin-disc stars with a mode at $(g - r)_0 \approx 0.38$ mag. On the other hand, the deepest gradient in this absolute magnitude interval, $d[\text{Fe}/\text{H}]/dZ = -0.187 \pm 0.013 \text{ dex kpc}^{-1}$, corresponds to the vertical distance interval $2 < Z \leq 5$ kpc. However it is rather close to the one in $0 < z \leq 2$ kpc, $d[\text{Fe}/\text{H}]/dZ = -0.176 \pm 0.022 \text{ dex kpc}^{-1}$. It seems that sufficient number of thin-disc stars lie up to vertical distance $Z = 5$ kpc.

Now, we will compare the vertical metallicity gradients estimated in this study with the ones in Table 4. We will prefer the star samples with high Galactic latitudes. Doing this, we will adopt the stars with the absolute magnitudes $5 < M_g \leq 6$ as thin-disc stars, and those with $4 < M_g \leq 5$ mag and $Z \leq 5$ kpc as thick-disc stars, while stars with $4 < M_g \leq 6$ mag will be adopted as the combination of two populations. For thin disc: the gradient in Schlesinger et al. (2014), $d[\text{Fe}/\text{H}]/dZ = -0.243^{+0.039}_{-0.053} \text{ dex kpc}^{-1}$ and one in Yaz & Karaali (2010), $d[\text{Fe}/\text{H}]/dZ = -0.320 \pm 0.010 \text{ dex kpc}^{-1}$ are both deeper than ours. For thick disc: the gradient in Ak et al. (2007a), $d[\text{Fe}/\text{H}]/dZ = -0.380 \pm 0.060 \text{ dex kpc}^{-1}$ is a bit deeper than $d[\text{Fe}/\text{H}]/dZ = -0.324 \pm 0.026 \text{ dex kpc}^{-1}$ in our study. The gradient in Karaali et al. (2003b), $d[\text{Fe}/\text{H}]/dZ = -0.200 \text{ dex kpc}^{-1}$ for thin and thick disc populations is compatible with the three gradients estimated for stars with absolute magnitudes $4 < M_g \leq 6$, $d[\text{Fe}/\text{H}]/dZ = -0.181 \pm 0.006$, $d[\text{Fe}/\text{H}]/dZ = -0.202 \pm 0.029$ and $d[\text{Fe}/\text{H}]/dZ = -0.196 \pm 0.010 \text{ dex kpc}^{-1}$.

Conclusion: Metallicity gradients are vertical distance and absolute magnitude dependent. The thin-disc stars cover the absolute magnitude interval $5 < M_g \leq 6$. Whereas the thick disc and halo stars share the absolute magnitudes $4 < M_g \leq 5$, i.e. apparently bright ones ($g_0 \leq 18$ mag) are thick-disc stars, while the faint stars ($g_0 > 18$ mag) are dominated by halo population.

6 Acknowledgments

We would like to thank the referee Dr. C. Du for useful and constructive comments concerning the manuscript. This work has been supported in part by the Scientific and Technological Research Council (TÜBİTAK) 114F347. Part of this work was supported by the Research Fund of the University of Istanbul, Project Number: 52265. This research has made use of the SIMBAD, and NASA's Astrophysics Data System Bibliographic Services.

References

- Ak, S., Bilir, S., Karaali, S., Buser, R., Cabrera-Lavers, A., 2007a, *NewA*, 12, 605
- Ak, S., Bilir, S., Karaali, S., Buser, R., 2007b, *AN*, 328, 169
- Alam, S., Albareti, F. D., Allende Prieto, C., et al., 2015, *ApJS*, 219, 12
- Bartaşüté, S., Aslan, Z., Boyle, R. P., 2003, *BaltA*, 12, 539
- Bensby, T., Feltzing, S., Oey, M. S., 2014, *A&A*, 562, A71
- Bilir, S., Karaali, S., Gilmore, G., 2006, *MNRAS*, 366, 1295
- Bilir, S., Cabrera-Lavers A., Karaali S., Ak S., Yaz E., López-Corredoira M., 2008a, *PASA*, 25, 69
- Bilir, S., Karaali, S., Ak, S., Yaz, E., Cabrera-Lavers, A., Coşkunoğlu, K. B., 2008b, *MNRAS*, 390, 1569
- Bilir, S., Ak, S., Karaali, S., Cabrera-Lavers, A., Chonis, T. S., Gaskell, C. M., 2008c, *MNRAS*, 384, 1178
- Bilir, S., Karaali, S., Ak, S., Coşkunoğlu, K. B., Yaz, E., Cabrera-Lavers, A., 2009, *MNRAS*, 396, 1589
- Chen, B., Stoughton, C., Smith, J. A., et al., 2001, *ApJ*, 553, 184
- Chonis, T. S., Gaskell, C. M., 2008, *AJ*, 135, 264
- Eggen, O.J., Lynden-Bell, D., Sandage, A.R., 1962, *ApJ*, 136, 748
- ESA, 1997, The Hipparcos and Tycho catalogues. Publisher: Noordwijk, Netherlands: ESA Publications Division 1997, Series: ESA SP Series vol no: 1200, ISBN: 9290923997
- Freeman, K., Bland-Hawthorn, J., 2002, *ARA&A*, 40, 487
- Helmi, A., Ivezić, Z., Prada, F., et al., 2003, *ApJ*, 586, 195
- Ivezic, Z., Sesar, B., Juric, M., et al., 2008, *ApJ*, 684, 287
- Juric, M., Ivezić, Z., Brooks, A., et al., 2008, *ApJ*, 673, 864
- Karaali, S., Bilir, S., Karataş, Y., Ak, S. G., 2003a, *PASA*, 20, 165
- Karaali, S., Ak, S. G., Bilir, S., Karataş, Y., Gilmore, G., 2003b, *MNRAS*, 343, 1013
- Karaali, S., Bilir, S., Hamzaoglu, E., 2004, *MNRAS*, 355, 307
- Karaali, S., Bilir, S., Tunçel, S., 2005, *PASA*, 22, 24
- Karaali, S., Bilir, S., Ak, S., Yaz, E., Coşkunoğlu, B., 2011, *PASA*, 28, 95
- Karataş, Y., Schuster, W., 2006, *MNRAS*, 371, 1793
- Kordopatis, G., Recio-Blanco, A., de Laverny, P., et al., 2011, *A&A*, 535, 107
- Laird, J. B., Carney, B. W., Latham, D. W., 1988, *AJ*, 95, 1843
- Mikolaitis, Š., Hill, V., Recio-Blanco, A., et al., 2014, *A&A*, 572, A33
- Nissen, P. E., Schuster, W. J., 1991, *A&A*, 251, 457
- Nissen, P. E., Schuster, W. J., 2010, *A&A*, 511L, 10
- Önal Taş, Ö., Bilir, S., Seabroke, G. M., Karaali, S., Ak, S., Ak, T., Bostancı, Z. F., 2016, *PASA*, 33, 44
- Peng, X., Du, C., Wu, Z., 2012, *MNRAS*, 422, 2756
- Phleps, S., Meisenheimer, K., Fuchs, B., Wolf, C., 2000, *A&A*, 356, 108
- Reddy, B. E., Lambert, D. L., Allende Prieto, C., 2006, *MNRAS*, 367, 1329
- Sandage, A., 1969, *ApJ*, 158, 1115
- Schlesinger, K. J., Johnson, J. A., Rockosi, C. M., et al., 2014, *ApJ*, 791, 112
- Searle, L., Zinn, R., 1978, *ApJ*, 225, 357
- Siegel, M. H., Majewski, S. R., Reid, I. N., Thompson, I. B., 2002, *ApJ*, 578, 151
- Tunçel Güçtekin, S., Bilir, S., Karaali, S., Ak, S., Ak, T., Bostancı, Z. F., 2016, *Ap&SS*, 361, 186
- Valenti, J. A., Fischer, D. A., 2005, *ApJS*, 159, 141
- van Leeuwen, F., 2007, *A&A*, 474, 653
- Venn, K. A., Irwin, M., Shetrone, M. D., et al., 2004, *AJ*, 128, 1177
- Yaz, E., Karaali, S., 2010, *NewA*, 15, 234
- York, D. G., Adelman, J., Anderson, J. E., et al., 2000, *AJ*, 120, 1579